THE JOURNAL OF PHYSICAL CHEMISTRY Letters

Letter

pubs.acs.org/JPCL

Discovery of Pb-Free Perovskite Solar Cells via High-Throughput Simulation on the K Computer

Takahito Nakajima* and Keisuke Sawada

Computational Molecular Science Research Team, RIKEN Advanced Institute for Computational Science, 7-1-26 minatojima-minami, Cyuo-ku, Kobe, Hyogo 650-0047, Japan

Supporting Information

ABSTRACT: We performed a systematic high-throughput simulation with density functional theory for 11 025 compositions of hybrid organic−inorganic halide compounds in ABX_3 and $A_2BB'X_6$ forms, where A is an organic or inorganic component, B/B′ is a metal atom, and X is a halogen atom. The computational results were compiled as a materials database. We performed massive computational simulation by using the K computer, which is a massively parallel many-core supercomputer in Japan. By applying the screening procedure to all the compounds in the materials database, we discovered novel candidates for environmentally friendly lead-free perovskite solar cells and propose 51 low-toxic halide single and double perovskites, most of which are newly proposed in this study. The proposed low-toxic halide double perovskites are classified under six families: group-14−group-14, group-13−group-15, group-11−group-11, group-9−group-13, group-11−group-13, and group-11−group-15 double perovskites.

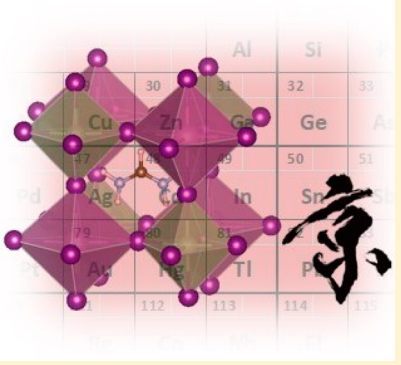

Hybrid organic−inorganic halide perovskites are one of the promising new-generation solar cells, which are expected to generate renewable resources and resolve global energy problems.[1−7] The power conversion efficiencies of perovskite photovoltaic-based devices rapidly increased from 3.8%[1] in 2009 to over 22%[8] in 2017 with further possibility of significant enhancement. The remarkable performances of hybrid halide perovskites in solar cells mainly originates from the excellent optical and electrical properties such as large absorption coefficients in the ultraviolet−visible spectral region, high carrier mobilities, long electron−hole diffusion lengths, and the direct band gap nature.

The most prominent and extensively studied hybrid halide perovskite in photovoltaic applications is a type of lead-based halide such as methylammonium lead iodide ($MAPbI_3$, MA = CH_3NH_3) and formamidinium lead iodide ($FAPbI_3$, FA = $HC(NH_2)_2$). These lead halide perovskites are easily synthesized and have a low production cost. However, their shortcomings such as chemical instability and toxicity need to be resolved. The hybrid lead halide perovskites contain heavy-metal Pb atoms, which are poisonous and harmful. Thus, it is desirable to search for novel hybrid lead-free halide perovskites containing nontoxic and widely available metals. Experimental and theoretical studies on lead-free perovskite solar cells are in progress. Comprehensive reviews on lead-free perovskite solar cells have appeared recently.[9−11]

Massive computational simulation can discover novel materials prior to experimental studies. In this study, we performed a systematic high-throughput computational simulation of hybrid organic−inorganic halide compounds including single and double perovskites, and discovered novel candidates for lead-free perovskite solar cells using the computational screening technique. In particular, we performed a more massive computational simulation compared to previous computational studies[12−16] by using the K computer, which is a massively parallel many-core supercomputer and has 88 128 nodes and 705 024 SPARC64 VIIIfx central processing unit (CPU) cores.

We considered compounds with ABX_3 and $A_2BB'X_6$ forms, where the molecular or atomic A = MA, FA, or Cs; metal B/B′ = Be, B, C, N, Mg, Al, Si, P, Ca, Sc, Ti, V, Cr, Mn, Fe, Co, Ni, Cu, Zn, Ga, Ge, As, Sr, Y, Zr, Nb, Mo, Tc, Ru, Rh, Pd, Ag, Cd, In, Sn, Sb, Ba, Hf, Ta, W, Re, Os, Ir, Pt, Au, Hg, Tl, Pb, or Bi; and halogen X = Cl, Br, or I. The total number of chemical compositions was 11 025. The computational results were compiled as a materials database. The database is available in the Excel sheet in the Supporting Information. All first-principles calculations were performed with the Vienna Ab initio Simulation Package (VASP).[17] The library was constructed as follows. The details are given in the Supporting Information.

1. The geometry and cell optimizations for all compositions of ABX_3 and $A_2BB'X_6$ were performed by scalar relativistic (SR) PBE functional with the width of the Gaussian smearing. After the optimized structures were obtained, we examined whether a system is metallic and excluded the metallic systems from the subsequent calculations. This step reduced the number of possible compounds from 11 025 to 2143. The structures of the

Received: August 21, 2017
Accepted: September 19, 2017
Published: September 19, 2017

DOI: 10.1021/acs.jpclett.7b02203
J. Phys. Chem. Lett. 2017, 8, 4826−4831

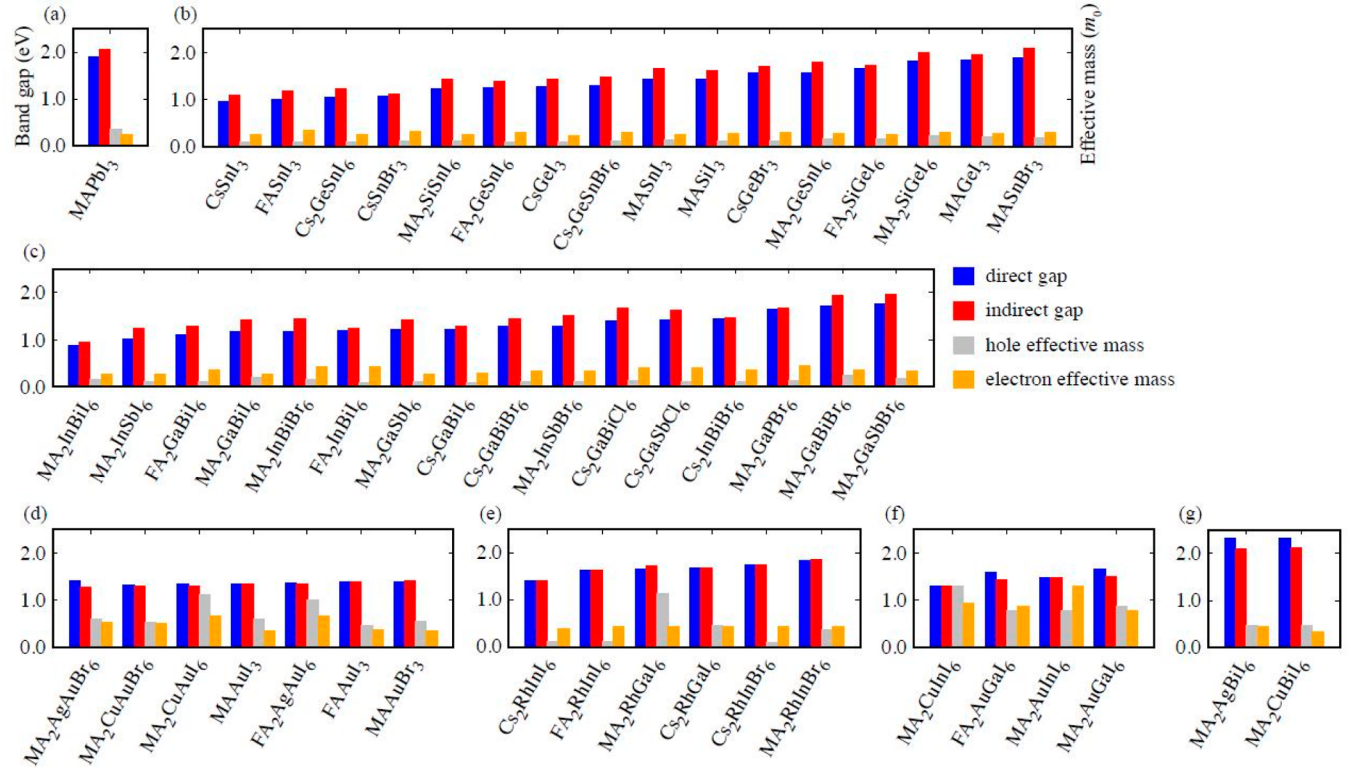

Figure 1. Direct and indirect band gaps (in eV) and hole and electron absolute effective masses (in m_0) for $MAPbI_3$ (a), group-14−group-14 (b), group-13−group-15 (c), group-11−group-11 (d), group-9−group-13 (e), group-11−group-13 (f), and group-11−group-15 (g) perovskites.

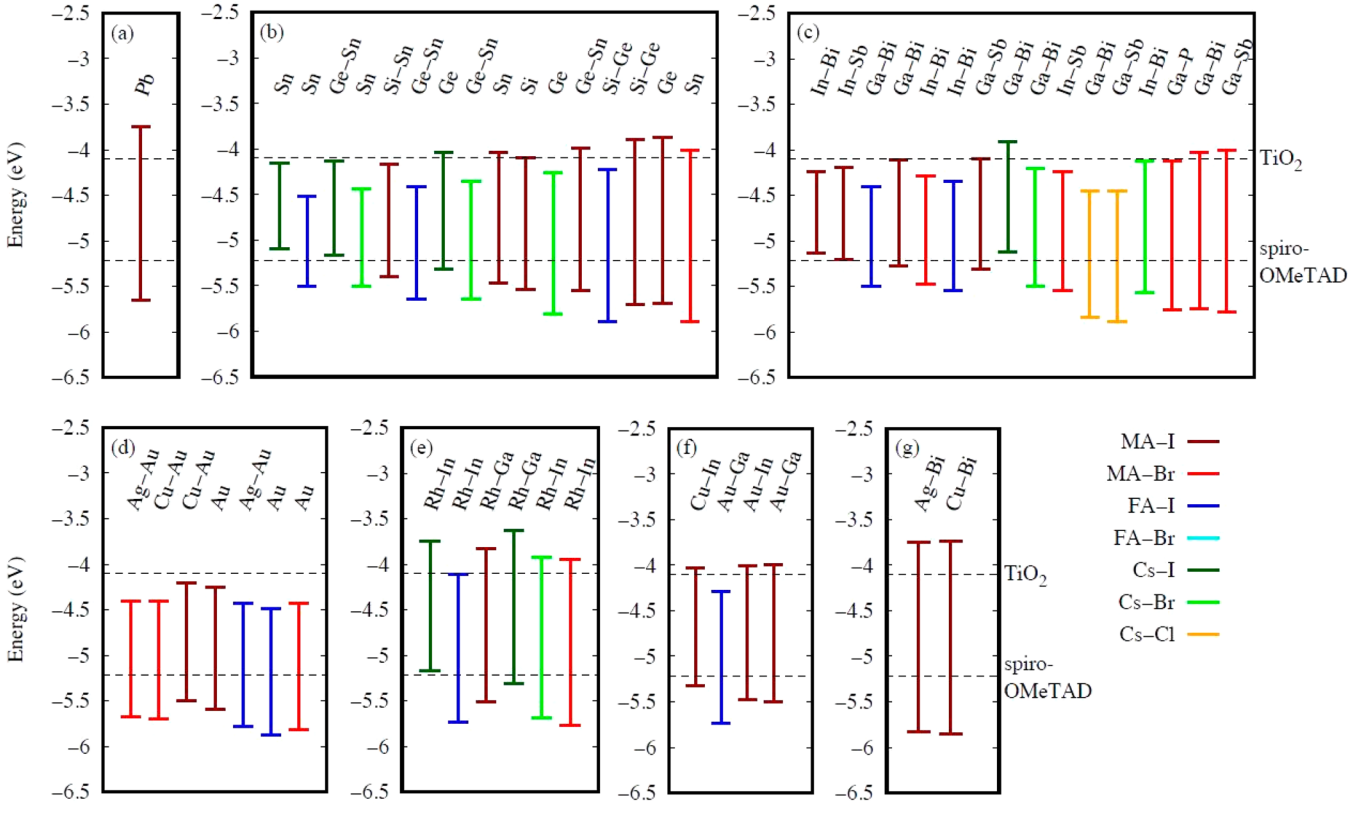

Figure 2. Positions of the band edges of VBM and CBM (in eV) for $MAPbI_3$ (a), group-14−group-14 (b), group-13−group-15 (c), group-11−group-11 (d), group-9−group-13 (e), group-11−group-13 (f), and group-11−group-15 (g) perovskites.

remaining compounds were reoptimized by the SR-PBE functional with no smearing scheme. The optimized structures of 2143 compounds are listed as POSCAR files of the VASP in the Supporting Information.

DOI: 10.1021/acs.jpclett.7b02203
J. Phys. Chem. Lett. 2017, 8, 4826−4831

Table 1. All Candidate Perovskites and Their Lowest Band Gaps (in eV)

group-14−group-14		group-13−group-15		group-11−group-11		group-11−group-13	
$CsSnI_3$	0.95	MA_2InBiI_6	0.88	$MA_2AgAuBr_6$	1.27	MA_2CuInI_6	1.29
$FASnI_3$	1.00	MA_2InSbI_6	1.01	$MA_2CuAuBr_6$	1.29	FA_2AuGaI_6	1.44
Cs_2GeSnI_6	1.04	FA_2GaBiI_6	1.10	MA_2CuAuI_6	1.30	MA_2AuInI_6	1.47
$CsSnBr_3$	1.07	MA_2GaBiI_6	1.16	$MAAuI_3$	1.34	MA_2AuGaI_6	1.50
MA_2SiSnI_6	1.22	$MA_2InBiBr_6$	1.18	FA_2AgAuI_6	1.35		
FA_2GeSnI_6	1.24	FA_2InBiI_6	1.19	$FAAuI_3$	1.38	group-11−group-15	
$CsGeI_3$	1.28	MA_2GaSbI_6	1.21	$MAAuBr_3$	1.39	MA_2AgBiI_6	2.09
$Cs_2GeSnBr_6$	1.29	Cs_2GaBiI_6	1.21			MA_2CuBiI_6	2.11
$MASnI_3$	1.43	$Cs_2GaBiBr_6$	1.29	group-9−group-13			
$MASiI_3$	1.44	$MA_2InSbBr_6$	1.29	Cs_2RhInI_6	1.42		
$CsGeBr_3$	1.56	$Cs_2GaBiCl_6$	1.39	FA_2RhInI_6	1.63		
MA_2GeSnI_6	1.56	$Cs_2GaSbCl_6$	1.43	MA_2RhGaI_6	1.67		
FA_2SiGeI_6	1.66	$Cs_2InBiBr_6$	1.45	Cs_2RhGaI_6	1.68		
MA_2SiGeI_6	1.82	MA_2GaPBr_6	1.64	$Cs_2RhInBr_6$	1.76		
$MAGeI_3$	1.83	$MA_2GaBiBr_6$	1.72	$MA_2RhInBr_6$	1.83		
$MASnBr_3$	1.89	$MA_2GaSbBr_6$	1.77				

2. After all the optimized structures were obtained, we examined whether the structures were perovskite or not in accordance with the criteria described in the Supporting Information.
3. The compounds with band gaps larger than 3.5 eV at the SR-PBE level were excluded from the subsequent procedure. This criterion reduced the number of possible compounds from 2143 to 1923.
4. For all of the remaining 1923 compounds, more accurate band gaps were evaluated by the hybrid HSE functional[18] with spin−orbit (SO) interactions. In this work, since the full SO-HSE calculation required demanding computational resources, approximate SO-HSE calculation was performed for total energy and band gap by an extension of the ONIOM extrapolation scheme[19,20] to the band calculation. An extended version of the HSE functional (HSE12)[21] was adopted in this study.
5. The hole and electron effective masses were further calculated for all the 1923 candidate compounds at the SR-PBE level.
6. The positions of the band edges of the valence band maximum (VBM) and the conduction band minimum (CBM) were further calculated for each candidate compound. An empirical scheme[22,23] was employed to evaluate the band edges.

To select typical candidates for efficient low-toxic organic−inorganic perovskite solar cells from the database, the following criteria were set:

A. The compounds with perovskite structure were retained.
B. The compounds with band gaps between 0.8 and 2.2 eV at the SO-HSE12 level were selected since the band gap of a typical good light absorber lies between 1.3 and 1.7 eV.[24,25]
C. Perovskites with direct band gaps were selected because a direct-gap material is capable of efficiently using strong photoabsorption in the thin film form and is beneficial as an efficient photovoltaic absorber. In addition, indirect-gap materials with small deviations (less than 0.25 eV in this work) from the lowest direct band gap value were also retained.
D. It is known that the charges in perovskite solar cells act as free holes and electrons rather than as excitons,[26] and have high mobility. Thus, perovskites with absolute values of hole and electron effective masses (m_h and $-m_e$, respectively) smaller than 1.5 m_0 were selected.
E. The compounds whose CBM ε_{CBM} and VBM ε_{VBM} satisfactorily match the CBM of the electron transport layer (ETL), ε_{CBM}^{ETL}, and the VBM of the hole transport layer (HTL), ε_{VBM}^{HTL}, respectively, were retained. In this study, TiO_2 and spiro-OMeTAD were adopted as typical electron and hole transport layers, respectively.
F. Since perovskites with low toxicity are desirable, compounds containing Pb, Hg, Cd, As, and Tl were rejected.

The above design criteria yielded 51 low-toxic single and double perovskites. All of the candidates are shown in Figures 1 and 2, and listed in Table 1. The results calculated for $MAPbI_3$ are also included in Figures 1 and 2 for side-by-side comparisons. The details of computational results are shown in Tables S1−S6 of the Supporting Information. When the screening criterion for toxicity (Criterion F) was ignored, 43 single and double perovskites were found additionally. Additional toxic perovskites are listed in Table S7 of the Supporting Information. Table S7 includes the typical perovskite photovoltaic materials such as $MAPbI_3$, $FAPbI_3$, and $CsPbI_3$, confirming that our screening procedure is reliable. The potential candidates for low-toxic perovskites are categorized as the following six types based on the combination of groups to which the B- and B′-site elements belong in the periodic table: group-14−group-14, group-13−group-15, group-11−group-11, group-9−group-13, group-11−group-13, and group-11−group-15 double perovskites. It should be noted that all of the identified mixed-double perovskites were newly discovered in this study.

The group-14−group-14 double perovskites are formed by the homovalent substitution of divalent lead cations with isovalent group-14 cations, which have the same electronic configuration as the lead cation does. Our screening procedure yielded nine and seven types of single and double perovskites, respectively, as potential candidates. The perovskites containing silicon, germanium, and/or tin atoms were retained, while those containing carbon atoms were rejected because the perovskite structures of the compounds containing carbon atoms are unstable. All the candidates of this family are desirable in terms of optical and carrier transport properties, as shown in Figure 1. These perovskites exhibit direct band gaps. Moreover, both the

DOI: 10.1021/acs.jpclett.7b02203
J. Phys. Chem. Lett. 2017, 8, 4826−4831

hole and electron effective masses for all the candidates are small and close to those calculated for $MAPbI_3$ (m_h = 0.36 m_0 and m_e = −0.25 m_0 in our calculation). From Figures S1−S3 of the Supporting Information, it is found that the VBM of $A_2BB'X_6$ is mainly dominated by the X-p orbitals, and slightly includes the s components of B and B′. The CBM of $A_2BB'X_6$ consists of the p states of B, B′, and X. These findings indicate that the bands around the VBM and CBM of these valence-isoelectronic compounds are almost independent of the A-site cations and d orbitals of the B-site cation. While the retained perovskites containing silicon, germanium, and/or tin cations are desirable in terms of optoelectronic and carrier transport properties, these perovskites may be unstable because Si^{2+}, Ge^{2+}, and Sn^{2+} cations can be easily oxidized to an oxidation state of +4. The solution for this instability is currently under investigation in many research groups.[9] When these compounds are rendered stable, the group-14−group-14 double perovskites proposed in this study can become the promising candidates for lead-free perovskite photovoltaic materials.

The group-13−group-15 double perovskites are valence-isoelectronic to the group-14 lead perovskites. Here, two divalent lead cations are replaced by a monovalent group-13 cation and a trivalent group-15 cation. Our screening procedure identified 16 types of group-13−group-15 double perovskites; one Ga−P, three Ga−Sb, six Ga−Bi, two In−Sb, and four In−Bi perovskites. All the candidates of group-13−group-15 double perovskites have direct band gaps and small carrier effective masses. The hole and electron effective masses of these candidates are close to those calculated for $MAPbI_3$. The comparison between Figures S4−S5 and Figure S1 indicates that the band structures and PDOSs around the VBM and CBM of group-13−group-15 double perovskites are also similar to those of the typical group-14 perovskite, $MAPbI_3$. Thus, the identified group-13−group-15 double perovskites are also expected to be promising candidates for lead-free perovskite photovoltaic materials.

The group-11−group-11 double perovskites are formed by a mixture of monovalent B and trivalent B′ metal cations.[9] Our screening procedure retained seven types of group-11−group-11 halide perovskites including group-11 single perovskites as potential candidates. All of these candidate compounds contain gold atoms. Most of the candidates exhibit indirect band gaps, while the differences between the lowest indirect and direct gaps are small for all the compounds. The hole and electron effective masses for this series of perovskites are larger than those calculated for $MAPbI_3$. As shown in Figure S6, the d orbitals of group-11 elements participate in both the VBM and CBM, which indicates that the carrier conductivities of group-11−group-11 perovskites differ from those of group-14−group-14 and group-13−group-15 perovskites. Further, since the band dispersions of VBM and CBM are not so large, the effective masses are relatively large; thus, it is expected that the carrier conductivities of group-11−group-11 perovskites are lower than those of $MAPbI_3$.

To our best knowledge, the group-9−group-13 double perovskites have not been reported, either experimentally or theoretically. Six kinds of group-9−group-13 double perovskites were selected by our screening procedure; four Rh−In and two Rh−Ga perovskites. Most of these candidates exhibit direct band gaps, while $Cs_2RhInBr_6$ has the indirect band gap. The difference between the lowest direct and indirect band gaps is small in all the candidates. The identified Rh−In double perovskites have small effective masses, while Rh−Ga double perovskites have relatively large masses. Consequently, it is expected that the charge carrier conductivities of Rh−In double perovskites are comparable to that of $MAPbI_3$. The group-9−group-13 double perovskites are valence-isoelectronic to the group-11−group-11 perovskites. Thus, the bands and PDOSs around the VBM and CBM of this family of perovskites are similar to those of the group-11−group-11 perovskites (see Figure S6). The identified Rh−In double perovskites can be one of the most promising candidates when their optical and carrier transport properties are considered. These double perovskites contain the expensive rhodium atoms. From our database, we could find an alternative $MA_2CoInCl_6$ that contains the inexpensive group-9 cobalt atoms, but which was excluded because its direct band gap of 2.27 eV was slightly large. The hole and electron effective masses of this perovskite are 0.21 and −0.55 m_0, respectively, which are comparable to those of $MAPbI_3$. Thus, we expect that replacing the organic or inorganic cation other than MA, FA, and Cs in the Co−In double perovskite will yield a promising inexpensive lead-free perovskite photovoltaic material.

We propose four kinds of group-11−group-13 double perovskites; one Au−In, two Au−Ga, and one Cu−In perovskites. The double perovskites containing indium atoms tend to have a direct-gap nature as compared to those containing gallium atoms. Among four group-11−group-13 double perovskites, MA_2CuInI_6 is desirable in terms of cost. The absolute values of effective masses of MA_2CuInI_6 are larger than those of $MAPbI_3$, which indicates that the carrier conductivities of MA_2CuInI_6 are relatively low. Interestingly, the total oxidation state of +4 for Cu−In in MA_2CuInI_6 is the same as that in $CuInSe_2$ (CIS) solar cells, while the crystal structures are different. Thus, further experimental and theoretical studies on the photovoltaic applications of this family of perovskites are valuable and necessary.

Since our calculation shows that the group-11−group-15 double perovskites have indirect and large band gaps, most of these compounds were removed from the candidate list. However, as the group-11−group-15 candidates with a small difference between the lowest indirect and direct band gaps, we propose two kinds of bismuth halide double perovskites. Since the hole and electron effective masses for the two perovskites are almost similar to those of $MAPbI_3$, it is predicted that the carrier mobilities are high in these candidates. The two identified group-11−group-15 perovskites have relatively large band gaps. Thus, it is expected that better photovoltaic absorbers based on group-11−group-15 double perovskites can be designed by substituting the A site other than MA, FA, and Cs.

In summary, by using the K computer, we performed a systematic high-throughput first-principles simulation of hybrid organic−inorganic halide compounds with the forms ABX_3 and $A_2BB'X_6$, where A is an organic or inorganic component, B/B′ is a metal atom, and X is a halogen atom, and constructed a materials library containing 11025 compositions. By screening the materials database according to structure, optical property, carrier conductivity, toxicity, and band alignment, we discovered novel candidates for lead-free perovskite solar cells. We proposed six families of novel low-toxic halide double perovskites: group-14−group-14, group-13−group-15, group-11−group-11, group-9−group-13, group-11−group-13, and group-11−group-15 double perovskites. We discovered 51 low-toxic halide single and double perovskites, which are newly proposed in this study except for the tin- and germanium-based

DOI: 10.1021/acs.jpclett.7b02203
J. Phys. Chem. Lett. 2017, 8, 4826−4831

single perovskites. The experimental and theoretical studies on the photovoltaic applications of lead-free halide double perovskites are in the nascent stage. To synthesize several halide double perovskites proposed in this study, instead of the one-step solution processing method or the vapor-assisted technique, new processing techniques that yield high-quality crystals at reasonable production costs may be developed. Several candidate compounds may not form large three-dimensional crystals, but like to form lower-dimensional perovskites with poor power conversion efficiency. To improve the efficiency for lower-dimensional perovskites, the hot spin-casting technique,[27] which creates layered perovskite crystals with near-single-crystalline quality, is one promising approach. In addition, the oxidation instability problem of several candidate perovskites should be resolved by further progresses in encapsulation techniques or chemical stabilization techniques. We hope that the candidate perovskites proposed in this study are synthesized and characterized experimentally so that several alternatives to the lead halide perovskites are obtained for photovoltaic applications. Moreover, the optimization of the A site and/or the X site in the compounds excluded from the candidates is expected to promote the development of novel and efficient low-toxic photovoltaic materials for practical applications.

Our further attempts are directed toward enhancing the materials library by adding other types of perovskites such as oxides and nitrides. We expect that our database can be used as an extensive materials library for potential applications other than photovoltaics such as light-emitting diodes, fuel cells, memory devices, field-effect transistors, thermoelectric conversion materials, and photocatalysts.

■ ASSOCIATED CONTENT

Supporting Information

The Supporting Information is available free of charge on the ACS Publications website at DOI: 10.1021/acs.jpclett.7b02203.

Details of computational conditions, high-throughput computation, and screening procedure; table listing the candidate perovskites; figures depicting the representative band structures and project densities of states; comparison with previous theoretical studies (PDF)

Computational materials databases (XLSX)

POSCAR files of VASP for the optimized structures of 2143 compounds (TXT)

■ AUTHOR INFORMATION

Corresponding Author

*E-mail: nakajima@riken.jp.

ORCID

Takahito Nakajima: 0000-0002-0229-3666

Notes

The authors declare no competing financial interest.

■ ACKNOWLEDGMENTS

This work was supported by the Next-Generation Supercomputer project (the K computer project) and FLAGSHIP2020 within the priority study 5 (Development of new fundamental technologies for high-efficiency energy creation, conversion/storage and use) of MEXT, Japan, FOCUS Establishing Supercomputing Center of Excellence, and the Creation of Innovative Functions of Intelligent Materials on the Basis of the Element Strategy from CREST, Japan Science and Technology (JST) Agency.

■ REFERENCES

(1) Kojima, A.; Teshima, K.; Shirai, Y.; Miyasaka, T. Organometal Halide Perovskites as Visible-Light Sensitizers for Photovoltaic Cells. *J. Am. Chem. Soc.* **2009**, *131*, 6050−6051.

(2) Park, N.-G. Organometal Perovskite Light Absorbers Toward a 20% Efficiency Low-Cost Solid-State Mesoscopic Solar Cell. *J. Phys. Chem. Lett.* **2013**, *4*, 2423−2429.

(3) Snaith, H. J. Perovskites: The Emergence of a New Era for Low-Cost, High-Efficiency Solar Cells. *J. Phys. Chem. Lett.* **2013**, *4*, 3623−3630.

(4) Green, M. A.; Ho-Baillie, A.; Snaith, H. J. The Emergence of Perovskite Solar Cells. *Nat. Photonics* **2014**, *8*, 506−514.

(5) Boix, P. P.; Nonomura, K.; Mathews, N.; Mhaisalkar, S. G. Current Progress and Future Perspectives for Organic/Inorganic Perovskite Solar Cells. *Mater. Today* **2014**, *17*, 16−23.

(6) Gao, P.; Gratzel, M.; Nazeeruddin, M. K. Organohalide Lead Perovskites for Photovoltaic Applications. *Energy Environ. Sci.* **2014**, *7*, 2448−2463.

(7) Brittman, S.; Adhyaksa, G. W. P.; Garnett, E. C. The Expanding World of Hybrid Perovskites: Materials Properties and Emerging Applications. *MRS Commun.* **2015**, *5*, 7−26.

(8) Yang, W. S.; Park, B.-W.; Jung, E. H.; Jeon, N. J.; Kim, Y. C.; Lee, D. U.; Shin, S. S.; Seo, J.; Kim, E. K.; Noh, J. H.; Seok, S. I. Iodide Management in Formamidinium-Lead-Halide−Based Perovskite Layers for Efficient Solar Cells. *Science* **2017**, *356*, 1376−1379.

(9) Hoefler, S. F.; Trimmel, G.; Rath, T. Progress on Lead-Free Metal Halide Perovskites for Photovoltaic Applications: A Review. *Monatsh. Chem.* **2017**, *148*, 795−826.

(10) Lyu, M.; Yun, J.-H.; Chen, P.; Hao, M.; Wang, L. Addressing Toxicity of Lead: Progress and Applications of Low-Toxic Metal Halide Perovskites and Their Derivatives. *Adv. Energy Mater.* **2017**, *7*, 1602512.

(11) Chakraborty, S.; Xie, W.; Mathews, N.; Sherburne, M.; Ahuja, R.; Asta, M.; Mhaisalkar, S. G. Rational Design: A High-Throughput Computational Screening and Experimental Validation Methodology for Lead-Free and Emergent Hybrid Perovskites. *ACS Energy Lett.* **2017**, *2*, 837−845.

(12) Castelli, I. E.; García-Lastra, J. M.; Thygesen, K. S.; Jacobsen, K. W. Bandgap Calculations and Trends of Organometal Halide Perovskites. *APL Mater.* **2014**, *2*, 081514.

(13) Filip, M. R.; Giustino, F. Computational Screening of Homovalent Lead Substitution in Organic−Inorganic Halide Perovskites. *J. Phys. Chem. C* **2016**, *120*, 166−173.

(14) Korbel, S.; Marques, M. A. L.; Botti, S. Stability and Electronic Properties of New Inorganic Perovskites from High-Throughput Ab Initio Calculations. *J. Mater. Chem. C* **2016**, *4*, 3157−3167.

(15) Jain, A.; Voznyy, O.; Sargent, E. H. High-Throughput Screening of Lead-Free Perovskite-Like Materials for Optoelectronic Applications. *J. Phys. Chem. C* **2017**, *121*, 7183−7187.

(16) Zhao, X.-G.; Yang, J.-H.; Fu, Y.; Yang, D.; Xu, Q.; Yu, L.; Wei, S.-H.; Zhang, L. Design of Lead-Free Inorganic Halide Perovskites for Solar Cells via Cation-Transmutation. *J. Am. Chem. Soc.* **2017**, *139*, 2630−2638.

(17) Kresse, G.; Furthmüller, J. Efficiency of Ab-Initio Total Energy Calculations for Metals and Semiconductors Using a Plane-Wave Basis Set. *Comput. Mater. Sci.* **1996**, *6*, 15−50.

(18) Heyd, J.; Scuseria, G. E.; Ernzerhof, M. Hybrid Functionals Based on a Screened Coulomb Potential. *J. Chem. Phys.* **2003**, *118*, 8207−8215.

(19) Humbel, S.; Sieber, S.; Morokuma, K. The IMOMO Method: Integration of Different Levels of Molecular Orbital Approximations for Geometry Optimization of Large Systems: Test for *n*-butane Conformation and S_N2 Reaction: RCl + Cl^-. *J. Chem. Phys.* **1996**, *105*, 1959−1967.

(20) Nakajima, T. An Extrapolation Scheme for Solid-State NMR Chemical Shift Calculations. *Chem. Phys. Lett.* **2017**, *677*, 99−106.

DOI: 10.1021/acs.jpclett.7b02203
J. Phys. Chem. Lett. 2017, 8, 4826−4831

(21) Moussa, J. E.; Schultz, P. A.; Chelikowsky, J. R. Analysis of the Heyd−Scuseria−Ernzerhof Density Functional Parameter Space. *J. Chem. Phys.* **2012**, *136*, 204117.
(22) Butler, M. A.; Ginley, D. S. Prediction of Flatband Potentials at Semiconductor-Electrolyte. Interfaces from Atomic Electronegativities. *J. Electrochem. Soc.* **1978**, *125*, 228−232.
(23) Xu, Y.; Schoonen, M. A. The Absolute Energy Positions of Conduction and Valence Bands of Selected Semiconducting Minerals. *Am. Mineral.* **2000**, *85*, 543−556.
(24) Shockley, W.; Queisser, H. J. Detailed Balance Limit of Efficiency of p-j Junction Solar Cells. *J. Appl. Phys.* **1961**, *32*, 510−519.
(25) Snaith, H. J. Estimating the Maximum Attainable Efficiency in Dye-Sensitized Solar Cells. *Adv. Funct. Mater.* **2010**, *20*, 13−19.
(26) D'Innocenzo, V.; Grancini, G.; Alcocer, M. J. P.; Kandada, A. R. S.; Stranks, S. D.; Lee, M. M.; Lanzani, G.; Snaith, H. J.; Petrozza, A. Excitons Versus Free Charges in Organo-Lead Tri-Halide Perovskites. *Nat. Commun.* **2014**, *5*, 3586−3591.
(27) Tsai, H.; Nie, W.; Blancon, J.-C.; Stoumpos, C. C.; Asadpour, R.; Harutyunyan, B.; Neukirch, A. J.; Verduzco, R.; Crochet, J. J.; Tretiak, S.; et al. High-Efficiency Two-Dimensional Ruddlesden−Popper Perovskite Solar Cells. *Nature* **2016**, *536*, 312−316.

DOI: 10.1021/acs.jpclett.7b02203
J. Phys. Chem. Lett. 2017, 8, 4826−4831